Contrasting effects of secondary organic aerosol formations on organic aerosol hygroscopicity

Ye Kuang[1,2], Shan Huang[1,2*], Biao Xue[1,2], Biao Luo[1,2], Qicong Song[1,2], Wei Chen[3], Weiwei Hu[3], Wei Li[1,2], Pusheng Zhao[4], Mingfu Cai[1,2], Yuwen Peng[1,2], Jipeng Qi[1,2], Tiange Li[1,2], Sihang Wang[1,2], Duohong Chen[5], Dingli Yue[5], Bin Yuan[1,2], Min Shao[1,2*]

[1] Institute for Environmental and Climate Research, Jinan University, Guangzhou, China.

[2] Guangdong-Hongkong-Macau Joint Laboratory of Collaborative Innovation for Environmental Quality, Guangzhou, China.

[3] State Key Laboratory of Organic Geochemistry and Guangdong Key Laboratory of Environmental Protection and Resources Utilization, Guangzhou Institute of Geochemistry, Chinese Academy of Sciences, Guangzhou 510640, China

[4] Institute of Urban Meteorology, China Meteorological Administration, Beijing 100089, China

[5] Guangdong Ecological and Environmental Monitoring Center, State Environmental Protection Key Laboratory of Regional Air Quality Monitoring, Guangzhou 510308, China

*Correspondence to: Shan Huang (shanhuang_eci@jnu.edu.cn) and Min Shao (mshao@pku.edu.cn)

Abstract

Water uptake abilities of organic aerosol under sub-saturated conditions play critical roles in direct aerosol radiative effects and atmospheric chemistry, however, field characterizations of organic aerosol hygroscopicity parameter κ_{OA} under sub-saturated conditions remain limited. In this study, a field campaign was conducted to characterize κ_{OA} at relative humidity of 80% with hourly time resolution for the first time in the Pearl River Delta region of China. Observation results show that during this campaign secondary organic aerosol (SOA) dominated total organic aerosol mass (mass fraction >70% on average), which provides ~~us~~ a unique opportunity to investigate influences of SOA formation on κ_{OA}. Results demonstrate that the commonly used organic aerosol oxidation level parameter O/C was weakly correlated with κ_{OA} and failed in describing the variations of κ_{OA}. However, the variations in κ_{OA} were well reproduced by mass fractions of organic aerosol factor resolved based on aerosol mass spectrometer measurements. The more oxygenated organic aerosol (MOOA) factor, exhibiting the highest average O/C (~1) among all organic aerosol factors, was the most important factor driving the increase of κ_{OA} and was commonly associated with regional air masses. The less oxygenated

organic aerosol (LOOA, average O/C of 0.72) factor, revealed strong daytime production, exerting negative effects on κ_{OA}. Surprisingly, the aged biomass burning organic aerosol (aBBOA) factor also formed quickly during daytime and shared a similar diurnal pattern with LOOA, but had much lower O/C (0.39) and had positive effects on κ_{OA}. The correlation coefficient between κ_{OA} and mass fractions of aBBOA and MOOA in total organic aerosol mass reached above 0.8. The contrasting effects of LOOA and aBBOA formation on κ_{OA} demonstrates that volatile organic compound (VOC) precursors from diverse sources and different SOA formation processes may result in SOA with different chemical composition, functional properties as well as microphysical structure, consequently, ~~exert~~exerting distinct influences on κ_{OA} and ~~render~~rendering single oxidation level parameters (such as O/C) unable to capture those differences. Aside from that, distinct effects of aBBOA on κ_{OA} was observed during different episodes, suggesting that the hygroscopicity of SOA associated with similar sources might also differ much under different emission and atmospheric conditions. Overall, these results highlight that it is imperative to conduct more researches on κ_{OA} characterization under different meteorological and source conditions, and examine its relationship with VOC precursor profiles and formation pathways to formulate a better characterization and develop more appropriate parameterization approaches in chemical and climate models.

1 Introduction

Organic aerosol (OA) composed of hundreds to thousands of organic species is one of the dominant aerosol components in the atmosphere and exert significant effects on climate and environment (Jimenez et al., 2009). The water uptake ability of atmospheric organic aerosol plays key roles in aerosol direct radiative effects and aerosol-cloud interactions (Rastak et al., 2017;Liu and Wang, 2010), and also aerosol liquid water content (Li et al., 2019;Jin et al., 2020) thus atmospheric chemistry. However, the hygroscopicity parameter κ_{OA} that describes the water uptake abilities of organic aerosol remains poorly quantified and mechanisms behind κ_{OA} variations are not well understood (Kuang et al., 2020b). Atmospheric OA is usually composed of both primary or secondary organic aerosol components. Primary OA (POA) is directly emitted from anthropogenic and natural sources such as biomass burning, coal and fossil fuel combustion, cooking and biogenic emissions.

Whereas secondary OA (SOA) is typically formed through atmospheric oxidation of volatile organic compounds (VOCs) or aging processes of POA. It is commonly thought that OA becomes more oxidized during its ~~evolvement~~evolution in the atmosphere and will in general be more hygroscopic after aging processes (Jimenez et al., 2009). A few studies have investigated the relationship between $\boldsymbol{\kappa_{OA}}$ and aerosol oxidation state parameters such as O/C ratio or f44 (fraction of m/z 44 in OA measurements of aerosol mass spectrometers). Some results, especially those from laboratory studies, demonstrated that $\boldsymbol{\kappa_{OA}}$ was highly correlated with O/C (Jimenez et al., 2009;Massoli et al., 2010;Kuang et al., 2020a;Zhao et al., 2016;Lambe et al., 2011), however, other researches demonstrated that $\boldsymbol{\kappa_{OA}}$ was not or only weakly correlated with O/C (Cerully et al., 2015;Lathem et al., 2013;Yeung et al., 2014;Alfarra et al., 2013). As the research continues, it was revealed that many factors can have significant impacts on $\boldsymbol{\kappa_{OA}}$, such as different functional groups, carbon chain length and aerosol liquid water content, etc. (Rickards et al., 2013;Suda et al., 2014;Petters et al., 2017;Marsh et al., 2017;Liu et al., 2018). Kuang et al. (2020b) recently reviewed laboratory and field measurements of $\boldsymbol{\kappa_{OA}}$ and concluded that O/C is not enough in parameterizing $\boldsymbol{\kappa_{OA}}$ and that additional parameters are needed. Therefore, it is worthwhile and imperative to endeavor on $\boldsymbol{\kappa_{OA}}$ quantifications and parametrizations, especially, considering that ~~organic aerosol~~OA might play more critical roles in atmospheric environment and climate for decades to come under strict control on anthropogenic emissions.

Most previous studies on $\boldsymbol{\kappa_{OA}}$ focused on laboratory studies, usually investigating $\boldsymbol{\kappa_{OA}}$ of SOA produced from laboratory chamber systems, which might be far different from real atmospheric SOA spectral. Quantifications of $\boldsymbol{\kappa_{OA}}$ based on field measurements remain relatively limited and are also urgently needed to yield complementary information, which in turn might provide guidance for the design of future laboratory studies. It is important to conduct more researches on $\boldsymbol{\kappa_{OA}}$ spatiotemporal distributions and examine its relationship with OA profiles to reach a better characterization and give rise to more appropriate parameterization approaches in chemical and climate models. China is a country that has been experiencing severe aerosol pollution and has been undergoing rapid changes under drastic air pollution control measures. However, despite the importance of organic aerosol hygroscopicity, only few studies attempted to quantify $\boldsymbol{\kappa_{OA}}$ based on field measurements (Wu et al., 2016;Li et al., 2019;Hong et al., 2018;Gunthe et al., 2011), mainly focusing on the North China Plain (NCP). The Pearl River Delta (PRD) region is much cleaner than the NCP in terms of particulate matter

pollution, suggesting that distinct regions in China are at different stages of air pollution controls (Xu et al., 2020). The composition of $PM_{2.5}$ (particulate matter with aerodynamic diameter less than 2.5 um) also differs much among regions, for example, OA and SOA fractions are much higher in the PRD than those in the NCP and their precursors are also much different (Zhou et al., 2020a). More investigations on κ_{OA} based on field studies in regions other than the NCP are urgently required.

In addition, most field studies on κ_{OA} only gave an estimate of the average κ_{OA} (Gunthe et al., 2011) or an average statistical relationship between κ_{OA} and O/C (Wu et al., 2013) and only few studies have reported κ_{OA} of higher time resolution featuring its diurnal variation characteristics (Deng et al., 2019), and almost no studies have reported κ_{OA} with high time resolution. Kuang et al. (2020a) proposed a new method to estimate κ_{OA} based on aerosol optical hygroscopicity measurements and bulk aerosol chemical composition measurements, which yielded κ_{OA} estimates at hourly time resolution. ~~Based on this dataset, it was found~~It revealed that variations in κ_{OA} were highly correlated with mass fractions of oxygenated organic aerosol in OA. In this study, the same method was applied to the dataset acquired from field measurements at a background site of the PRD region. High time resolution characterization of κ_{OA} and aerosol chemical properties were also achieved, which enabled us to dig deeper on what factors other than O/C drove the variations of κ_{OA} and to further elucidate on the complexity and possible approaches in parameterizing κ_{OA} based on field measurements. ~~Details~~We described details on aerosol measurements and the κ_{OA} estimation method ~~were presented~~ in ~~Sect.2~~measurements and ~~Sect.3, respectively. An~~method part. In the results and discussion section, we first sketched out the overview of campaign ~~data and general factors driving aerosol chemistry was presented in Sect 4.1. The variations in estimated~~measurements and then discussed the κ_{OA} ~~and its relationship to OA oxidation state~~variation characteristics as well as its influencing factors, and ~~to distinct OA factors were presented and discussed in Sect 4.2. The~~in the last part, the complexity regarding κ_{OA} parameterization was further demonstrated and elucidated ~~in Sect 4.3.~~. The summaries are provided in the conclusion part.

2 Measurements

2.1 Sampling site

Physical, optical and chemical properties of ambient aerosol particles as well as meteorological parameters and gas pollutants such as CO, O_3, and NO_x were continuously measured during autumn

(from 30th September to 17th November 2018) at a rural site in Heshan county, Guangdong province, China. This site ~~locates~~was located at a small mountain (22°42'N, 112°55'E, altitude of 55 m), about 55 km away from the megacity Guangzhou and ~~is~~was surrounded by villages and small residential towns and thus ~~is~~was little influenced by local industrial sources. The location of this site is ~~also~~ shown in Fig.S1. This site is also a supersite operated by the provincial environmental monitoring authority, therefore provides qualified meteorological parameters and pollutants measurements such as $PM_{2.5}$, CO, O_3 and NOx . Acetonitrile was measured by a proton transfer reaction time-of-flight mass spectrometer (PTR-ToF, Ionicon Analytik GmbH, Innsbruck, Austria).

2.2 Aerosol physical properties measurements

During this field campaign, instruments were placed in an air-conditioned room. Two inlets were housed on the roof of the three-floors building for aerosol sampling and both inlets ~~are~~were about 1.8 m above the floor. One of the inlets was a PM_{10} impactor with a 1.8 m-long Nafion drier that lowers the sample relative humidity (RH) down to less than 30% placed downstream of it. A flow splitter was placed below the drier and instruments downstream of this splitter ~~include~~included an Aerodynamic Particle Sizer (APS, TSI Inc., Model 3321, flow rate of 5 L/min), which measured the size distribution of ambient aerosol particles of aerodynamic diameter about 600 nm to 20 μm; an AE33 aethalometer (Drinovec et al., 2015) with a flow rate of 5 L/min, which ~~measures~~measured aerosol absorption coefficients at seven wavelengths; a humidified nephelometer system with a flow rate of about 6 L/min. The total flow rate of these instruments was about 16 L/min, which was quite close to the flow rate of 16.7 L/min required by the PM_{10} impactor. Thus, these instruments measured the physical and optical properties of PM_{10} particles.

The humidified nephelometer system ~~is~~was a laboratory self-assembled one, including two Aurora 3000 nephelometers. One nephelometer ~~measures~~measured the aerosol scattering properties (scattering and back scattering coefficients at three wavelengths: 450 nm, 525 nm, 635 nm) at a reference RH (called dry Nephelometer because ~~of~~the sampling RH is lower than 30%), and another nephelometer ~~measures~~measured the aerosol scattering properties under a fixed RH of 80% (called wet Nephelometer and the actual sampling RH fluctuates within ~~±~~±1%). Details on the humidifier and control algorithm ~~can~~could be found in Kuang et al. (2020a). ~~Note that to~~To make sure the accuracy

of the measured RH in the sensing volume of the wet Nephelometer, three Vaisala HMP110 sensors ~~with accuracies of~~ (±0.2 ℃ and ±1.7 % for RH between 0 to 90~~%~~%) were used to monitor the RH at different parts of the wet nephelometer. Two sensors were placed at the inlet and outlet of the wet nephelometer, one was placed in the sensing volume. The water vapor pressure calculated from these three sensors must be strictly consistent with each other (relative difference between any two of the sensors must be less than 2 %). Then the sampling RH of the wet nephelometer was calculated using the averaged water vapor pressure and the sample temperature measured by the sensor placed in the sensing volume of the wet nephelometer.

Another inlet was connected with a $PM_{2.5}$ impactor (BGI SCC2.354, cut diameter of 2.5 μm with a flow rate of 8 L/min) and was also equipped with a Nafion drier lowering the sampling RH down to less than 30%. Downstream of this inlet were a soot particle aerosol mass spectrometer (SP-AMS, Aerodyne Research, Inc., Billerica, MA, USA) and a scanning mobility particle sizer (SMPS; TSI model 3080), which measured the particle number size distribution (PNSD) ranging from 10 nm to 760 nm.

2.3 SP-AMS measurements and data analysis

The SP-AMS was deployed to measure the size-resolved chemical composition for submicron aerosol particles. The SP -AMS is ~~basically~~ a high-resolution time-of-flight aerosol mass spectrometer (HR-ToF-AMS) combining a laser vaporization device, i.e., soot particle (SP) mode. The instrument principle has been provided in previous papers (Canagaratna et al., 2007;Onasch et al., 2012). In brief, HR-ToF-AMS containing a tungsten vaporizer can provide information of those particulate species vaporized under around 600℃. By adding a Nd:YAG (1064nm) laser module inside of the HR-ToF-AMS, the vaporizing temperature can increase to around 4000℃, enabling the SP-AMS to detect refractory compositions such as black carbon (BC) and metals. After vaporized, the gaseous components ~~are~~were ionized in electron impact (70eV) way and then quantitatively measured by a time-of-flight mass spectrometer. ~~Controlled~~The air flow in the AMS was first controlled by the orifice ~~as well as~~and then focused through the aerodynamic lens of SP-AMS, and then particles with diameter in ~~submicrometer~~sub-micrometer range ~~are measured~~were detected. During the Heshan Campaign, SP-AMS was located next to a SMPS to minimize the sampling discrepancy. The SP-AMS alternately

switched between the V-mode (only tungsten vaporizer) and SP-mode (laser and tungsten vaporizer). The original time resolution of SP-AMS data was 1 min (per run), and ~~15min~~15 min average values were used in this study to avoid disturbance from mode switching. During the campaign, the calibration system for SP-AMS was not available and we used the values of ionization efficiency (IE) and relative ionization efficiency (RIE) of different species from the latest successful calibration. The applied RIEs for default SP-AMS species are: 1.1 for nitrate, 4 for ammonium, 1.2 for sulfate, 1.4 for organics and 1.3 for chloride. The composition dependent collection efficiency (CDCE) was applied to mentioned species following the instruction of Middlebrook et al.(2012). Refractory BC from SP-AMS was calculated by mass concentration of family C_x ions from high resolution mass spectrometer times a scaling factor (8) derived by comparison with equivalent BC mass concentration from AE33. SP-AMS data evaluation was performed by specific software Squirrel (v1.61) for unit mass resolution and Pika (v1.21) for high resolution based on Igor Pro (v6.37, WaveMetrics, Inc., Oregon, USA). Aside from the good consistency between the aerosol from derived from SMPS and SP-AMS components as mentioned in Sect.3.2~~,~~ (Fig.S5), the resulting mass concentrations from SP-AMS were further validated by consistency with the results from external measurements in the same site, e.g., offline $PM_{2.5}$ filter measurements and online measurements for total $PM_{2.5}$ mass and individual components using gas aerosol collection system (GAC) with ion chromatography~~.~~ operated (Figure S7, S8, and S9). More details of SP-AMS data quality assurance will be provided in a parallel paper (Huang et al., in preparation).

The source apportionment of organic aerosols (OA) was performed by positive matrix factorization (PMF) based on high resolution OA data collected in V-mode (only tungsten vaporizer). ~~As a wildly used source analysis method,~~The principle of PMF has been described in previous papers (Paatero, 1997;Paatero and Tapper, 1994). ~~PMF using AMS data can be conducted by an Igor Pro-based panel, i.e., PMF Evaluation Tool (PET, v2.06, Ulbrich et al., 2009). We input the matrices for OA mass concentration and uncertainty into the model and operated it according to the instruction in Ulbrich et al. (Ulbrich et al., 2009).~~In this study, PMF using high resolution AMS data including two matrices (organic ion mass concentrations and their uncertainties) were conducted by an Igor Pro-based panel, i.e., PMF Evaluation Tool (PET, v2.06, Ulbrich et al., 2009), following the instruction in Ulbrich et al. (2009). Isotopes and ions with m/z >120 were excluded to minimize the interference from repeatedly calculated uncertainties and noise signals. In total, 454 ions were considered in PMF.

After investigating different solutions with factor number from 2 to 10, a six-factor solution was chosen based on the best performance shown by PMF quality parameters and most reasonable source identification. Two primary OA factors were identified including a hydrocarbon-like OA (HOA, containing cooking emissions) and a biomass burning OA (BBOA). The other four factors were related to secondary formation or ageing process: 1) more oxygenated OA (MOOA, regional transport), 2) less oxygenated OA (LOOA, related to daytime photochemical formation), 3) nighttime-formed OA (Night-OA), and 4) aged BBOA (aBBOA). The mass spectral profile and time series of OA factors were shown in ~~Figure S3~~Fig.S6, and OA factors with identified sources will be discussed in Set. 4. More details on PMF solution selection and source identification will be provided in a parallel paper (Huang et al., in preparation).

3 Methodology

3.1 Aerosol hygroscopicity derivation from aerosol light scattering measurements

The aerosol light scattering enhancement factor $f(\mathrm{RH},\lambda)=\frac{\sigma_{sp}(RH,\ \lambda)}{\sigma_{sp}(dry\ \lambda)}$, $\sigma_{sp}(RH,\ \lambda)$ is the aerosol scattering coefficient at light wavelength of λ and condition of RH, and was only measured at 80% RH. Thus, the aerosol hygroscopicity parameter $\kappa_{f(\mathrm{RH})}$ was derived from $f(80\%, 525\ \mathrm{nm})$. ~~The principle of this method is to find~~ and $\kappa_{f(\mathrm{RH})}$ represents a diameter independent hygroscopicity parameter κ that fits the observed $f(80\%, 525\ \mathrm{nm})$ best and solved through iteration algorithm. Although Kuang et al. (2017) proposed a simple method for deriving $\kappa_{f(\mathrm{RH})}$ based only on measurements of the humidified nephelometer system, in this study, the more traditional method described therein was adopted to retrieve $\kappa_{f(\mathrm{RH})}$, which uses measurements of PNSD as inputs of Mie theory and the κ-Köhler theory. The idea of deriving $\kappa_{f(\mathrm{RH})}$ from aerosol light scattering measurements was first proposed by Chen et al. (2014), however, the physical understanding of $\kappa_{f(\mathrm{RH})}$ was not mathematically interpreted until the study of Kuang et al. (2020a). Briefly, $\kappa_{f(\mathrm{RH})}$ can be approximately understood as the overall hygroscopicity of aerosol particles with aerosol scattering coefficient contribution as the weighting function for size-resolved κ distribution. Results of Kuang et al. (2020a) demonstrated that for typical continental aerosols $\kappa_{f(\mathrm{RH})}$ represents the overall hygroscopicity of aerosol particles with a dry diameter range between 200 and 800 nm, thus no matter

if $\kappa_{f(\mathrm{RH})}$ values were retrieved based on aerosol light scattering enhancement factor measurements downstream of a PM_{10} or a PM_1 impactor, they are almost the same, which was confirmed by direct measurements in Kuang et al. (2020a) (observed average relative difference about 3.5%).

3.2 Organic aerosol hygroscopicity derivation based on aerosol chemical composition and optical hygroscopicity measurements

~~Aerosol~~The aerosol hygroscopicity parameter κ ~~were usually~~can be calculated ~~using measured~~ from aerosol chemical composition ~~based~~ measurements (κ_{chem}) on the basis of volume mixing rule ~~(κ_{chem}) to represent~~, thus the organic aerosol hygroscopicity ~~of aerosol particles of certain diameters or present the overall hygroscopicity of the entire~~ parameter κ_{OA} were usually estimated through closure between measured κ and estimated κ using aerosol ~~populations of PM1~~chemical measurements. In this study, the size-resolved aerosol chemical compositions of PM_1 were measured using the SP-

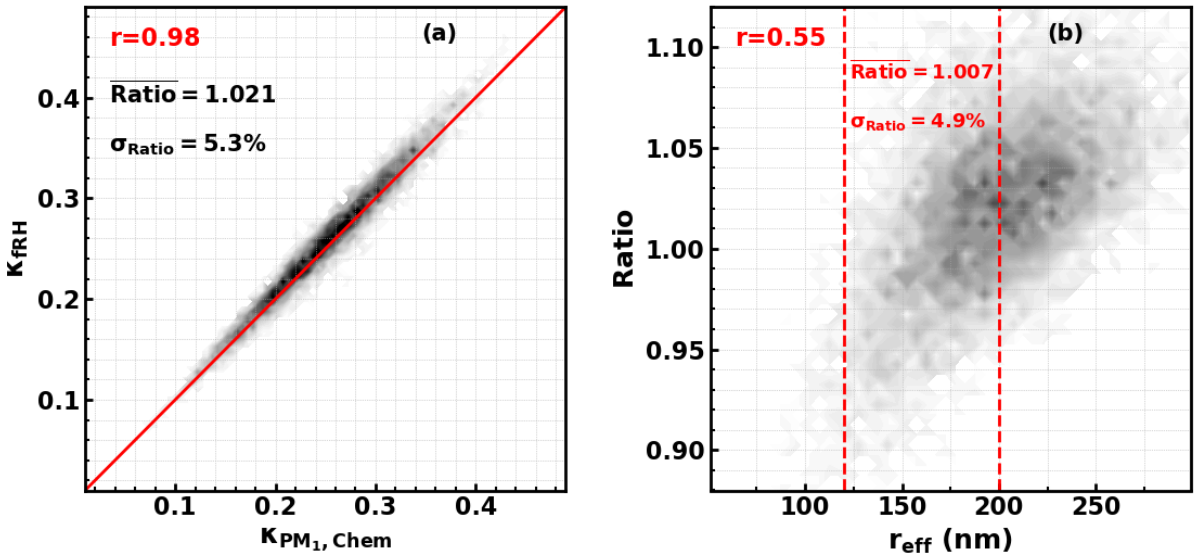

Figure 1. Simulated κ_{chem,PM_1} and $\kappa_{f(\mathrm{RH}),PM_{10}}$, red texts give correlation coefficients, Ratio=$\kappa_{f(\mathrm{RH}),PM_{10}}/\kappa_{chem,PM_1}$, r_{eff} is the effective radius of the aerosol populations, dashed red lines show the r_{eff} range during the field campaign of this study.

AMS, however, the overall aerosol hygroscopicity was only derived based on aerosol light scattering measurements of PM_{10} bulk aerosols. Results of Kuang et al. (2020a) demonstrated that κ_{chem} calculated based on bulk chemical compositions of PM_1 are quite consistent with $\kappa_{f(\mathrm{RH})}$ of PM_1 (κ_{chem,PM_1}) therefore also consistent with $\kappa_{f(\mathrm{RH})}$ of PM_{10}. ~~We have simulated~~ ($\kappa_{f(\mathrm{RH}),PM_{10}}$).

However, simulation results in Kuang et al. (2020a) demonstrated that the ~~$\kappa_{f(RH)}$ of PM_{10} and κ_{chem} of PM_1 under different PNSDs coupled with different~~ ratio between κ_{chem,PM_1} and $\kappa_{f(\mathrm{RH}),PM_1}$ varies with PNSD and size-resolved κ ~~distribution scenarios, as~~distributions, and the applicability of this conclusion under varying aerosol chemical compositions and size distributions need further clarification. Thus, we have designed a simulation experiments, to simulate the ratio between κ_{chem,PM_1} and $\kappa_{f(\mathrm{RH}),PM_{10}}$ considered wide ranges of aerosol chemical compositions and size distributions, details of the simulation are introduced in Part 2 of the supplement. The simulated results are shown in Fig.~~S2a. As shown in the results in Fig.S2b, $\kappa_{f(RH)}$ of PM_{10} and κ_{chem} of PM_1 are quite close to each other and the simulated~~1. The results shows that the average relative difference $(\frac{\kappa_{f(\mathrm{RH}),PM_{10}}-\kappa_{chem,PM_1}}{\kappa_{chem,PM_1}} \times 100\%)$ was ~~-0.4±3%. Thus, $\kappa_{f(RH)}$ of PM_{10} was used as the measured κ_{chem}~~ 2.1 ± 5.3%, which demonstrates that in general $\kappa_{f(\mathrm{RH}),PM_{10}}$ can be used to represent κ_{chem,PM_1} under varying atmospheric conditions. The results also show that the ratio=$\kappa_{f(\mathrm{RH}),PM_{10}}/\kappa_{chem,PM_1}$ is positively correlated with the effective radius of the aerosol population, which means that different levels of bias may exist under different PNSD conditions, and for effective radius range of this field campaign, the average relative difference is 0.7±4.9%. Given this, we have further simulated the $\kappa_{f(\mathrm{RH})}$ of PM_{10} and κ_{chem} of PM_1 under different PNSDs of this campaign coupled with different size-resolved κ distribution scenarios (as shown in Fig.S4a). As shown in the results in Fig.S4b, κ_{chem,PM_1} and $\kappa_{f(\mathrm{RH}),PM_{10}}$ are quite close to each other and the simulated average relative difference was -0.4±3%. Thus, $\kappa_{f(\mathrm{RH}),PM_{10}}$ was used as the measured κ_{chem,PM_1} in the following discussions.

The SP-AMS measures size-resolved PM_1 mass concentrations of SO_4^{2-}, NO_3^-, NH_4^+, Cl^- and organic aerosol, thus provides their bulk mass concentrations. A simplified ion pairing scheme was used to derive mass concentrations of different inorganic salts (as listed in Tab.1) based on measured bulk ion mass concentrations (Gysel et al., 2007;Wu et al., 2016). Note that the hygroscopicity parameter was measured at RH of 80%, the κ values of ammonium sulfate and ammonium nitrate at 80% RH were predicted using the Extended Aerosol Inorganic Model (E-AIM), whose predictions for ammonium nitrate and ammonium sulfate has been proven to be consistent with laboratory results

(Luo et al., 2020;Jing et al., 2018), and those of potassium chloride and ammonium bisulfate were consistent with Liu et al. (2014)

Table 1. Densities (ρ) and hygroscopicity parameters (κ) of inorganic salts used in this study

Species	NH_4NO_3 (AN)	NH_4HSO_4 (ABS)	$(NH_4)_2SO_4$ (AS)	KCl (PC)
ρ (g cm^{-3})	1.72	1.78	1.769	1.98
κ	0.56	0.56	0.56	0.89

Note that Cl^- was coupled with K^+ due to that biomass burning events prevailed during this field campaign. The simple volume mixing rule called Zdanovskii–Stokes–Robinson (ZSR) was usually used for $\boldsymbol{\kappa_{chem}}$ calculations, that is, bulk $\boldsymbol{\kappa_{chem}}$ of PM_1 can be calculated on the basis of volume fractions of different compounds ~~(ε_i)~~ (Petters and Kreidenweis, 2007) using the following equation:

$$\kappa_{chem} = \sum_i \kappa_i \cdot \varepsilon_i \qquad (1)$$

~~And~~Where κ_i ~~and ε_i are~~ is hygroscopicity parameter κ ~~and~~ of compound *i*, and ε_i is volume fraction of compound *i* in the mixture~~.~~ (V_i/Vtot, V_i and Vtot are volume of compound *i* and total aerosol volume of PM_1). Based on Eq.2 and Tab,1, κ_{chem} can be formulated as follows:

$$\kappa_{chem} = \kappa_{AS}\varepsilon_{AS} + \kappa_{AN}\varepsilon_{AN} + \kappa_{ABS}\varepsilon_{ABS} + \kappa_{PC}\varepsilon_{PC} + \kappa_{BC}\varepsilon_{BC} + \kappa_{OA}\varepsilon_{OA} + \kappa_X\varepsilon_X \qquad (2)$$

where κ_{OA} and ε_{OA} are κ and volume fraction of entire organic aerosol populations，κ_X and ε_X are κ and volume fraction of aerosol constituents which are beyond the detection ability of the SP-AMS. ~~The hygroscopicity of these~~These unidentified aerosol species, in continental regions, likely be dust but still possible composed of other components such as biogenic primary aerosol~~, were not discussed before.~~. On the basis of current literature reports, dust is nearly ~~hydrophilic~~hydrophobic and varies a lot, with κ of mineral dust and road dust as well as oil or coal fly ash are in the range of 0.01 to 0.08 (Koehler et al., 2009;Peng et al., 2020). In this paper, the unidentified part is assumed as dust and κ_X is arbitrarily specified as 0.05. The ε_X are estimated as the PM_1 volume concentration ($V_{tot,PM1}$) difference between measured by the SMPS and calculated from volume concentration summation of chemical compounds listed in Tab.1 and volume concentrations of BC and organic aerosol, and the estimated average contribution ε_X during this campaign is 13% as shown in Fig.~~S4~~S6. In the volume concentration calculations of BC and organic aerosol, BC density of 1.7 g/cm^3 was assumed, and

organic aerosol density is calculated based on the density parameterization shame proposed by Kuwata et al. (2012) using the organic aerosol elemental ratios O:C and H:C measured by the SP-AMS as input parameters. In addition, κ_{BC} was set to zero due to the ~~hydrophilic~~hydrophobic property of BC particles. Then, κ_{OA} can be estimated based on measured $\boldsymbol{\kappa_{chem}}$ using the following formula:

$$\kappa_{OA} = \frac{\kappa_{chem} - (\kappa_{AS}\varepsilon_{AS} + \kappa_{AN}\varepsilon_{AN} + \kappa_{ABS}\varepsilon_{ABS} + \kappa_{PC}\varepsilon_{PC} + \kappa_X\varepsilon_X)}{\varepsilon_{OA}} \quad (3)$$

The effects of κ_{chem} perturbations, aerosol mass concentrations, $V_{tot,PM1}$ as well as κ_X perturbations on κ_{OA} derivations are simulated using Monte-Carlo method for each data point of the κ_{OA} time series (1000 cases are randomly produced for each κ_{OA} data point) and average effects are summarized in Table 2. The perturbation parameter of κ_{chem} is based on the simulation results using PNSDs of this field campaign shown in Fig.S4. The perturbation parameters of aerosol mass concentrations are consistent with Hong et al. (2018), and that of $V_{tot,PM1}$ is from Ma et al. (2011). The perturbation parameter of κ_X is specified based on that κ of dust in general ranges from 0.01 to 0.08. The results show that the accuracy of using $\kappa_{f(\mathrm{RH}),PM_{10}}$ to represent κ_{chem,PM_1} affects most on κ_{OA} derivations.

Table 2. Effects of parameter perturbations on κ_{OA} derivations using Eq.3

Parameter	Uncertainty (3 standard deviations)	κ_{OA} variations (1 standard deviation)
SO_4 mass concentration	20%	0.01
NO_3 mass concentration	20%	0.006
NH_4 mass concentration	20%	0.002
OA mass concentration	20%	0.003
$\boldsymbol{\kappa_{chem}}$	9%	0.014
$V_{tot,PM1}$	25%	0.003
κ_X	0.03	0.003

4 Results and discussions

4.1 Overview of the campaign data

The time series of meteorological parameters such as wind speed, wind direction, RH and ambient air temperature, aerosol scattering coefficients, aerosol hygroscopicity parameter $\kappa_{f(\mathrm{RH})}$, mass concentrations of aerosol components as well as gas pollutant concentrations are shown in Fig.~~1~~2. During this campaign, the RH mainly ranged from 50% to 80% with an average (± 1σ) of 60±14%, with the nighttime RH frequently reached beyond 70%, which favors the nighttime aqueous phase chemistry. Temperatures mainly ranged from 18 to 28 ℃, with an average (± 1σ) of 23.6±3.3 ℃, indicating a relatively warm state during this campaign though in the autumn. The aerosol scattering coefficients at 525 nm ($\sigma_{sp,525}$) shown in Fig.~~1b~~2b demonstrate $\sigma_{sp,525}$ generally ranged between 20 to 600 Mm^{-1}, with an average (± 1σ) of 256±102 Mm^{-1}, indicating moderately polluted conditions during this campaign. The ~~NR-PM1~~non-refractory mass concentrations of PM_1 ($NR\text{-}PM_1$) measured by the SP-AMS ranged from 1 to 94 $\mu g/m^3$, with an average (± 1σ) of 33±14 $\mu g/m^3$. Nitrate, sulfate,

ammonium and organic aerosol contributed on average 19%, 11%, 9% and 58% to total NR-PM_1, which was consistent with the aerosol chemical compositions typically observed in the PRD region

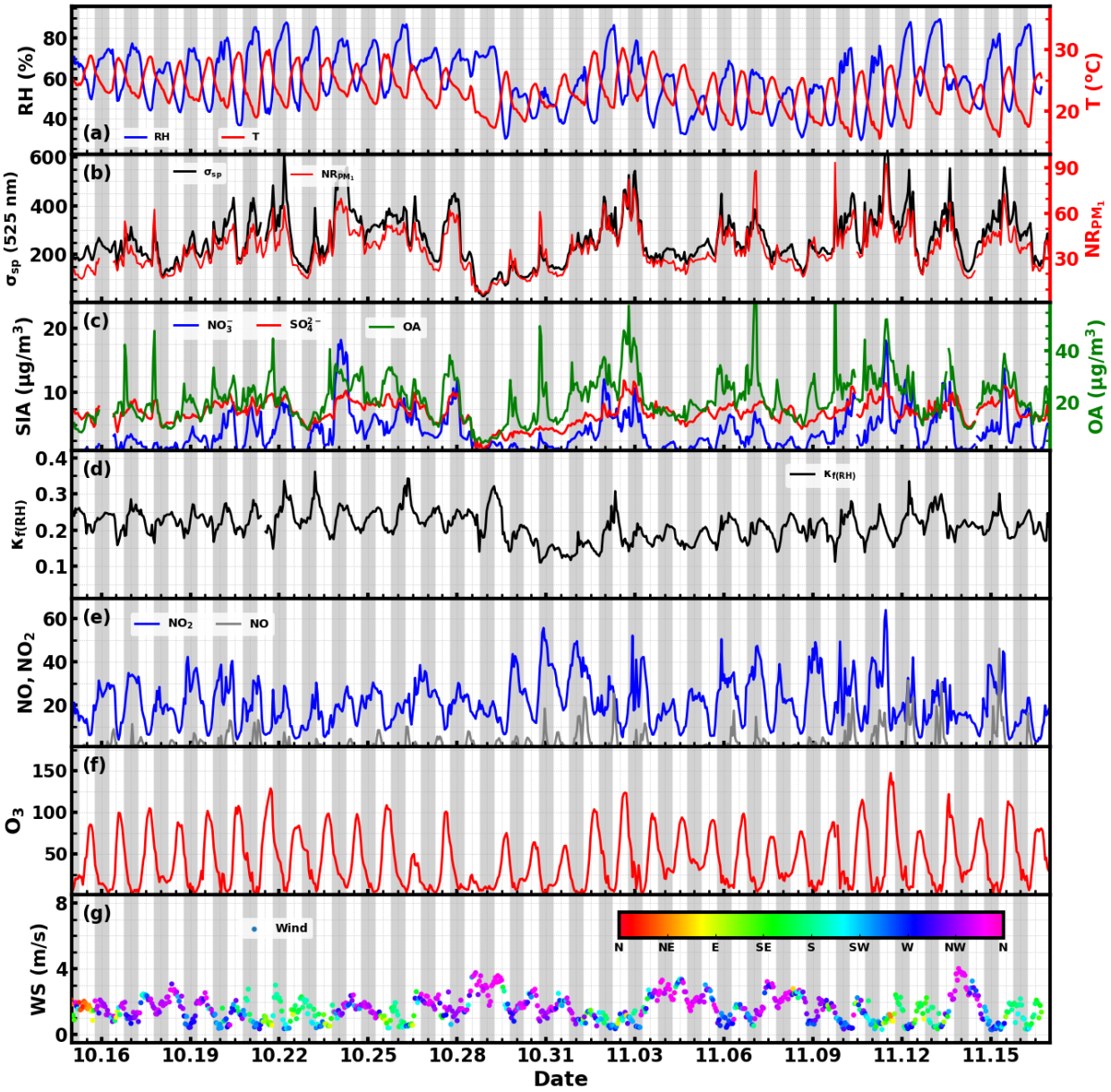

Figure 2. Time series of **(a)** RH and temperature; **(b)** aerosol scattering coefficient at 525 nm and mass concentrations of PM_1 non-refractory components; **(c)** mass concentrations of sulfate, nitrate and organic aerosol; **(d)**The hygroscopicity parameter κ retrieved from aerosol light scattering enhancement measurements; **(e)** NO and NO_2 concentrations; **(f)** O_3 concentration; **(g)** wind speed/direction. Shaded gray areas corresponding to nighttime periods.

featuring organic aerosol as the major constituent of NR-PM_1 and higher sulfate concentration than nitrate concentration (Zhou et al., 2020b). However, the NR-PM_1 composition profile differed much from those recently observed in urban Guangzhou (Guo et al., 2020), a megacity about 100 km away

from Heshan, where sulfate concentrations were on average only slightly higher than nitrate concentrations during autumn and winter seasons of 2017. The large mass contribution of organic aerosol in PM_1 resulted in generally moderate ambient aerosol hygroscopicity, with $\kappa_{f(RH)}$ ranging between 0.11 and 0.36 with an average (± 1σ) of 0.22±0.04. The small standard deviation further suggests for relatively small variations in aerosol hygroscopicity. Sulfate concentrations showed much less daily and diurnal variations than those of nitrate and organic aerosol, suggesting that the sulfate level was determined by the regional scale background, while nitrate and organic aerosol concentration were significantly influenced by local production. Especially, the nitrate concentration usually experienced a sharp increase since sunset and peaks after mid night, sometimes even reached beyond sulfate mass concentration. The time series of NO_2, NO and O_3 concentration are also shown in Fig.~~1e~~2e and Fig.~~1f~~2f. NO_2 concentration showed distinct diurnal variations, and ranged from 3.5 to 64 ppb with an average (± 1σ) of 20.5±10.5 ppb. The NO concentration ranged from almost 0 to 45 ppb with an average (± 1σ) of 2.2±4.5 ppb, indicating generally low concentrations of NO. O_3 concentrations ranged from 2 to 147 ppb with an average (± 1σ) of 41.5±31.4 ppb, frequently reaching over 90 ppb in the afternoon, indicating for strong daytime photochemistry, and dropped rapidly after sunset towards a very low concentration (usually below 5 ppb) after midnight.

The average diurnal variations of NO_2, NO, O_3, CO, aerosol chemical compositions, $\kappa_{f(RH)}$ and meteorological parameters are shown in Fig.~~2~~3. O_3 concentrations began to increase after sunrise, peaked near 15:00 and then began to decrease quickly but drops slower after midnight. Meanwhile, NO concentration began to decrease quickly after sunrise, reached and remained near zero after noontime, and began to slightly increase after 21:00. NO_2 concentration increased quickly after 15:00 and reached a plateau after 21:00. Variation characteristics of NO, O_3, and NO_2 suggest that the relatively low NO concentration resulted in weak titration effects on O_3, where upon typical NO_3 chemistry and subsequent N_2O_5 chemistry ~~was likely to occur, which was likely the mechanism behind the observed nitrate variations. Nitrate concentrations increased quickly since 16:00 and peaked after~~

~~midnight (about 03:00 LT), further confirming this speculation.~~ might occur, which might contribute

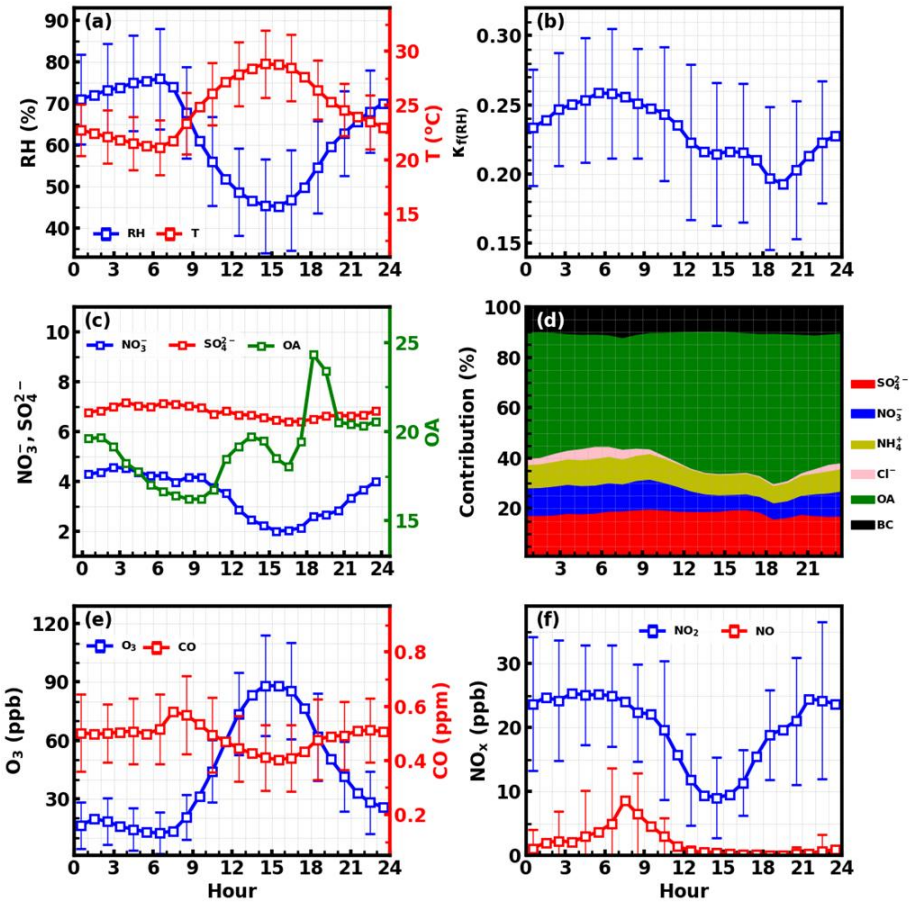

Figure 3. Average diurnal variations of **(a)** RH and T; **(b)** $\kappa_{f(RH)}$; **(c)** sulfate, nitrate and organic aerosol; **(d)** mass fractions of different components; **(e)** O_3 and CO; **(f)** NO_2 and NO.

to the observed nitrate increase after sunset. However, nitrate concentrations increased quickly after about 16:00 LT and peaked after midnight (about 03:00 LT), indicating that there must be a mechanism responsible for the observed nitrate increase at least before sunset. To dig more into this, the possible pathways of nitrate formation since 16:00 was simulated and discussed in Sect.3 of the supplement. The results demonstrate that the repartitioning of HNO_3 in gas and aerosol phase due to the temperature decrease and RH increase can mainly explain the observed nitrate increase. And the strong daytime photochemistry and decrease of NO_2 concentration might result in significant production of gas phase before about 16:00. However, the possible contribution of N_2O_5 hydrolysis to nitrate formation cannot be excluded.

Under the strong daytime photochemistry and nighttime ~~heterogenous formation~~increase of

nitrate, evident diurnal variations of aerosol hygroscopicity was observed. The overall aerosol hygroscopicity variation was generally consistent with the variation pattern of inorganic aerosol fraction in NR-PM_1 as shown in Fig.~~2d~~3d. In detail, the overall variations of nitrate and associated ammonium, as well as organic aerosol determines the general hygroscopicity variation pattern: the quick increase in organic aerosol between 16:00 to 19:00 resulted in the quick $\kappa_{f(\mathrm{RH})}$ decrease during this period; since then the general decrease of organic aerosol and increase of nitrate resulted in the increase of $\kappa_{f(\mathrm{RH})}$ until the next morning; the daytime decrease of nitrate and increase of organic aerosol resulted in a $\kappa_{f(\mathrm{RH})}$ decrease before 13:00. Note that sulfate concentration remaining almost constant throughout the day further confirmed previous statement that local production likely contributed less to sulfate concentration, which can be an indicator of regional air mass status.

These results suggest that ~~both~~typical strong daytime photochemistry and nighttime NO_3 chemistry characteristics occurred during this field campaign and played significant roles in diurnal variations of organic aerosol and nitrate, while aged regional air mass determined the sulfate concentration, which provides a good opportunity for investigating how typical daytime photochemistry and nighttime ~~NO_3~~ chemistry and aged regional organic aerosol components impact on organic aerosol hygroscopicity.

4.2 κ_{OA} derivations and its relationship with organic aerosol oxidation state

The organic aerosol hygroscopicity parameter κ_{OA} was derived according to the method mentioned in Sect.3.2, and the results with hourly time resolution are shown in Fig.~~3a~~4a. κ_{OA} revealed daily and diurnal variations, and ranged from almost zero to 0.28 with an average (± 1σ) of 0.085±0.05. The relationship between κ_{OA} and O/C was further investigated and shown in Fig.~~3b~~4b. Results demonstrated that κ_{OA} and O/C were weakly correlated during this campaign, with most data points falling in the published κ_{OA} and O/C relationship band. During this campaign, O/C generally resided in a small range (from about 0.4 to 0.6) with an average (± 1σ) of 0.~~053~~53±0.~~006~~06, indicating small variations in O/C, however, featuring drastic variations in κ_{OA}. The average diurnal variations of O/C and κ_{OA} are shown in Fig.~~3c~~4c. On average, κ_{OA} increased slowly during the nighttime and varied even smaller during most of the daytime. Nevertheless, it experienced a relatively quicker decrease from 17:00 to 19:00, which appeared to be coincident with the quick OA concentration increase as shown in Fig.~~2~~3. However, the O/C increased during the period when O_3 concentration

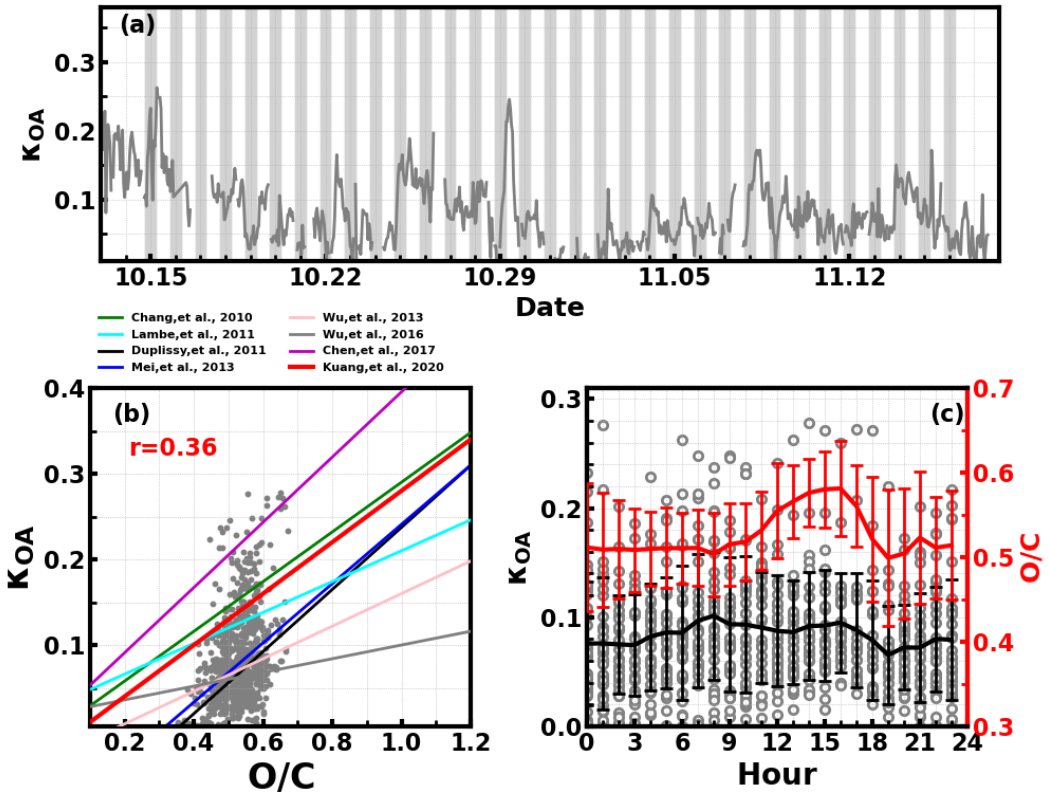

Figure 4. **(a)** Time series of derived κ_{OA}; **(b)** Correlations between O/C ratio and κ_{OA}, lines correspond to empirical relationships between κ_{OA} and O/C ratio reported in different studies; **(c)** Diurnal variations of κ_{OA} and O/C ratio;

increased quickly, suggesting that daytime photochemistry drove the OA oxidation during daytime. The key point here is that the diurnal patterns of O/C and κ_{OA} differed much from each other, which is why the variation in O/C failed to describe that of κ_{OA}.

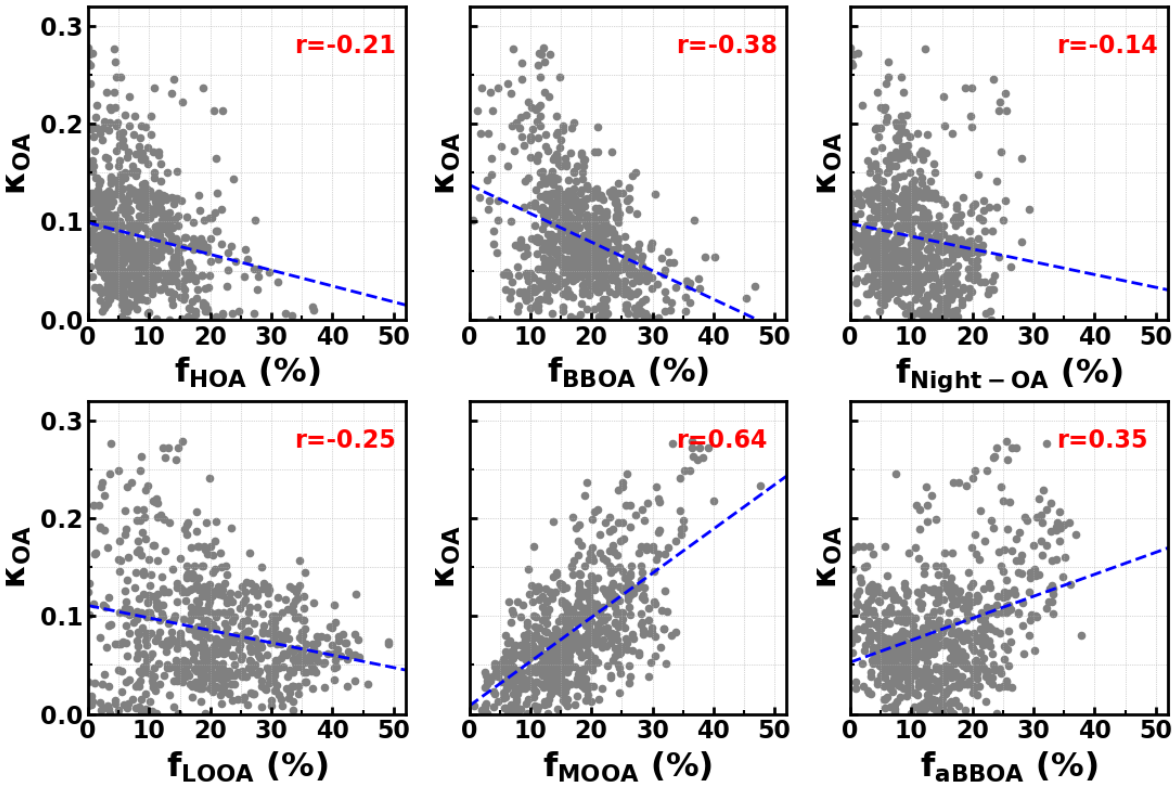

Figure 5. Correlations between κ_{OA} and mass fractions of OA factors in total OA mass.

The question remains which factors were controlling the variations of κ_{OA}. The relationships between κ_{OA} and mass fractions of different PMF OA factors in total OA mass were further investigated and shown in Fig.~~4~~5. In general, the average (± 1σ) mass fractions of HOA, BBOA, aBBOA, LOOA, Night-OA, and MOOA were: 8.7% (± 7.8%), 16.5% (± 8.3%), 15.9% (± 10.5%), 19.1% (± 10.9%), 10.4% (± 6.5%), 18.6% (± 12.2%), and it means that during this campaign SOA dominates organic aerosol (SOA > 70%). Two primary OA factors, HOA and BBOA were related to vehicle exhausts mixed with cooking emissions and to biomass burning emissions, respectively. κ_{OA} was negatively correlated with both HOA and BBOA, which is consistent with previous literature reports that primary OA components such as ~~HOA and BBOA are generally hydrophobic. The average diurnal variations of OA PMF factors shown in Fig.5~~HOA and BBOA are generally hydrophobic

(Kuang et al., 2020b). The average diurnal variations of OA PMF factors shown in Fig.6 demonstrate that both BBOA and HOA peaked near 18:00, which should be associated with the frequently observed biomass burning events and supper cooking in villages near the site. This explained the sharp increase of OA mass and the sharp decrease of κ_{OA} near 18:00 as shown in Fig.~~3c. It was generally thought that secondary aerosol formation would result in increases of aerosol hygroscopicity.~~6c. However, κ_{OA} was also negatively correlated with LOOA (Fig.~~4d~~5d), whose mass concentration increase rapidly after sunrise and are likely secondary due to local photochemistry with potential precursors ~~such as isoprene~~of both biogenic and anthropogenic VOCs~~.~~ considering the observation site is surrounded by small towns and areas with high percentage cover of trees (Fig.S1). The ~~average O/C ratio for~~ negative correlation between κ_{OA} and LOOA is ~~0.72, which is only lower than~~contradictory

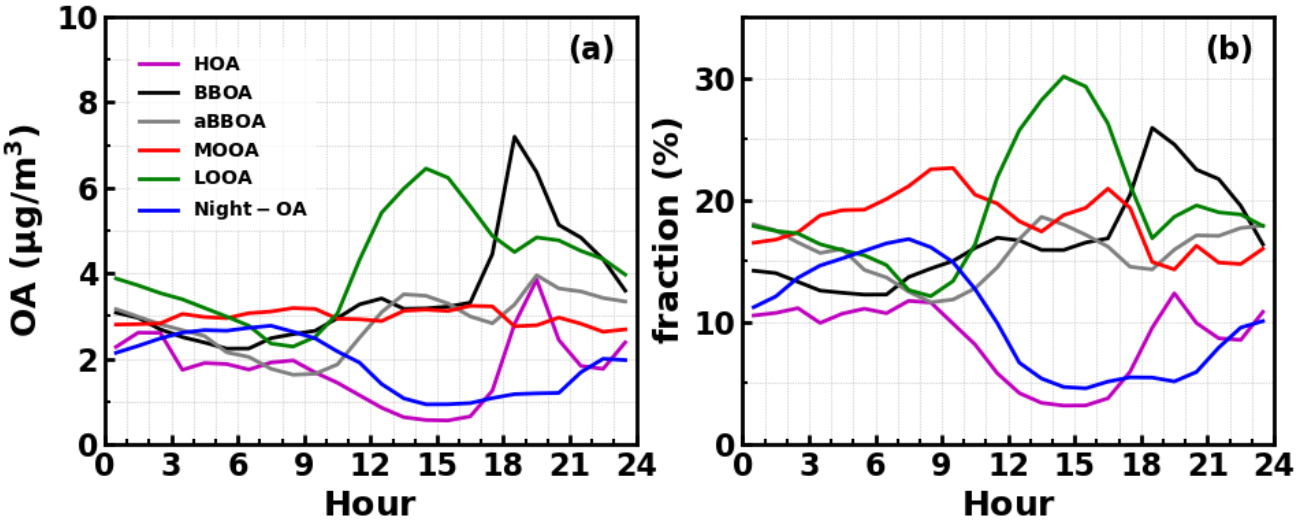

Figure 6. Average diurnal variations of mass concentrations **(a)** and their mass fractions **(b)** in total OA mass of different PMF OA factors.

with the generally thought that ~~of MOOA, suggesting that the daytime OOA~~secondary aerosol formation ~~and decrease of BBOA and HOA mass concentrations drove the increase~~would result in increases of ~~daytime O/C, and the~~aerosol hygroscopicity. The negative correlation between κ_{OA} and LOOA mass fraction explained why O/C failed to describe diurnal variations of κ_{OA}~~.~~: the O/C ratio for LOOA is 0.72, which is only lower than that of MOOA, suggesting that the daytime LOOA formation and decrease of BBOA and HOA mass concentrations drove the increase of daytime O/C but the κ_{OA} did not follow. The κ_{OA} was also negatively correlated with Night-OA fraction, which increased during nighttime ~~and~~(Fig.6). The Night-OA factor was highly correlated with nitrate concentrations (Figure ~~S4), which were~~S5), likely associated with the NO_3 nighttime chemistry as discussed in Sect. 4.1. Results of Suda et al. (2014) demonstrated that the addition of NO_3 radical

would exert negative impacts on κ_{OA}, ~~which is~~ consistent with the observations shown here. As shown in Fig.~~4~~5, κ_{OA} was positively correlated with both MOOA and aBBOA, especially with that of MOOA. MOOA was highly correlated with sulfate and showed almost no diurnal variations, indicating that the highly oxygenated (O/C ~1) MOOA was also more associated with regional air masses. The observed small nighttime increase of κ_{OA} could be associated with the slight increase in MOOA mass fraction as shown in Fig.~~5b~~6b. Similar to LOOA, the aBBOA increased during daytime, which revealed quick ~~ageing~~aging process of biomass burning related precursors or primary aerosols through photochemistry. Also, the aBBOA factor showed similar variation trend with $C_6H_2NO_4^+$ (m/z 151.998, see Fig. ~~S3~~S5) which ~~is~~was found as a characteristic ion of a typical aged BBOA component nitrocatechol (Bertrand et al., 2018). However, the resolved average O/C ratio of aBBOA was only 0.39, which is even lower than that of BBOA (O/C ~ 0.48), implying that BBOA were likely formed through oxidation of gaseous BBOA precursors rather than the direct oxidation of BBOA. The fact that nitrocatechol is more likely to be contributed by oxidation of gaseous precursors in biomass burning plumes rather than primary biomass burning emissions (Wang et al., 2019) rationalizes this speculation. The similar diurnal characteristics but contrasting effects of LOOA and aBBOA on κ_{OA} further explains the weak correlation coefficient between κ_{OA} and O/C. However，the weak but positive correlation between κ_{OA} and O/C should have arose from the much stronger positive correlation between κ_{OA} and MOOA mass fractions. LOOA has relatively high O/C and its abundance usually reaches above that of MOOA during the afternoon, however, its negative effects on κ_{OA} was partially compensated by aBBOA which had lower O/C. In addition, κ_{OA} was mostly associated with mass fractions of MOOA with highest O/C, thus giving rise to the weak but positive relationship between κ_{OA} and O/C. As for κ_{OA} diurnal variations, daytime increase of aBBOA and LOOA has compensating effects on κ_{OA}, and the HOA and Night-OA decrease further complicated its variations.

To test if effects of parameter perturbations on κ_{OA} derivations have significant effects on the relationships between κ_{OA} and organic aerosol PMF factors, we impose random perturbations on parameters listed in Table 2 in each κ_{OA} derivation. The comparison between originally derived κ_{OA} and perturbed derivation of κ_{OA} results is shown in Fig.S10. The average difference between derived κ_{OA} with and without random errors is 0, and the standard deviation is 0.03. However, the relationships between κ_{OA} derived with random errors and organic aerosol PMF factors changed only

a little bit, and the results are shown in Fig.S11.

4.3 Discussions on complexity of organic aerosol hygroscopicity parameterizations

As demonstrated in Sect.4.2, the LOOA factor with higher O/C had negative impacts on $\boldsymbol{\kappa_{OA}}$, while aBBOA with much lower O/C had positive effects on $\boldsymbol{\kappa_{OA}}$. These results suggested that O/C is not enough for parameterizing $\boldsymbol{\kappa_{OA}}$ and the question remains what additional parameters are needed or how should they be implemented~~?~~. To further explore on this issue, the relationships between $\boldsymbol{\kappa_{OA}}$ and mass fractions of aBBOA+MOOA in total OA mass ($f_{MOOA+aBBOA}$) was further investigated to manifest the complexity of $\boldsymbol{\kappa_{OA}}$ variations and discuss potential impact factors, with results shown in Fig.~~6a~~7a. As discussed in Sect.4.2, both MOOA and aBBOA had positive effects on $\boldsymbol{\kappa_{OA}}$, however, the relationship between $\boldsymbol{\kappa_{OA}}$ and $f_{MOOA+aBBOA}$ does not yield a higher correlation coefficient than that between $\boldsymbol{\kappa_{OA}}$ and f_{MOOA}, and the results shown in Fig.~~6a~~7a demonstrate that $\boldsymbol{\kappa_{OA}}$ and $f_{MOOA+aBBOA}$ might have different relationships during different periods. The relationships between $\boldsymbol{\kappa_{OA}}$ and $f_{MOOA+aBBOA}$ during three periods were further investigated and shown in Fig.~~6b~~7b-d, which shows that during the first period from 10-12 to 10-22, $\boldsymbol{\kappa_{OA}}$ was highly correlated with $f_{MOOA+aBBOA}$ (R=0.82), with all points falling in a narrow band, suggesting that $f_{MOOA+aBBOA}$ alone could describe the variations in $\boldsymbol{\kappa_{OA}}$ well. However, during the second period (from 10-23 to 11-02) and the third period (from 11-03 to 11-17) the correlation coefficients between $\boldsymbol{\kappa_{OA}}$ and $f_{MOOA+aBBOA}$ were much lower. Obviously, $f_{MOOA+aBBOA}$ during the second and the third period was in general much lower than that during the first period. The timeseries of $\boldsymbol{\kappa_{OA}}$ and different PMF OA factors are shown in Fig.~~7~~8. MOOA displayed relatively small variations during this campaign, highlighting that the regional air mass did not experience tremendous variations, and suggesting that changes of other OA factors especially aBBOA have resulted in different relationships between $\boldsymbol{\kappa_{OA}}$ and $f_{MOOA+aBBOA}$. The results in Fig.~~7c~~8c shows that the ratio between aBBOA and BBOA differs much during three periods and declines from the first period to the third period. During the first period, aBBOA was more abundant and was well correlated (R= 0.57) with BBOA. At the same time, aBBOA was positively correlated with HOA (R = 0.49) especially with the cooking emission tracer $C_6H_{10}O^+$ (R = 0.60), which could be emitted together with biomass burning emissions, when residents in surrounding villages cooked with biomass fuels. BBOA and aBBOA had comparable levels during the second period, however, aBBOA concentration

was much lower than that of BBOA during the third period. It can also be noticed that aBBOA in the second period showed higher correlation with BBOA (R = 0.45) than that in the last period (R = 0.17), which was also the case with cooking emission tracer (R = 0.60 for the 2nd period, 0.36 for the 3rd period). These results suggest that the chemical and physical properties of aBBOA likely changed much within the three periods despite similarities in PMF analysis. Both the primary gas pollutants

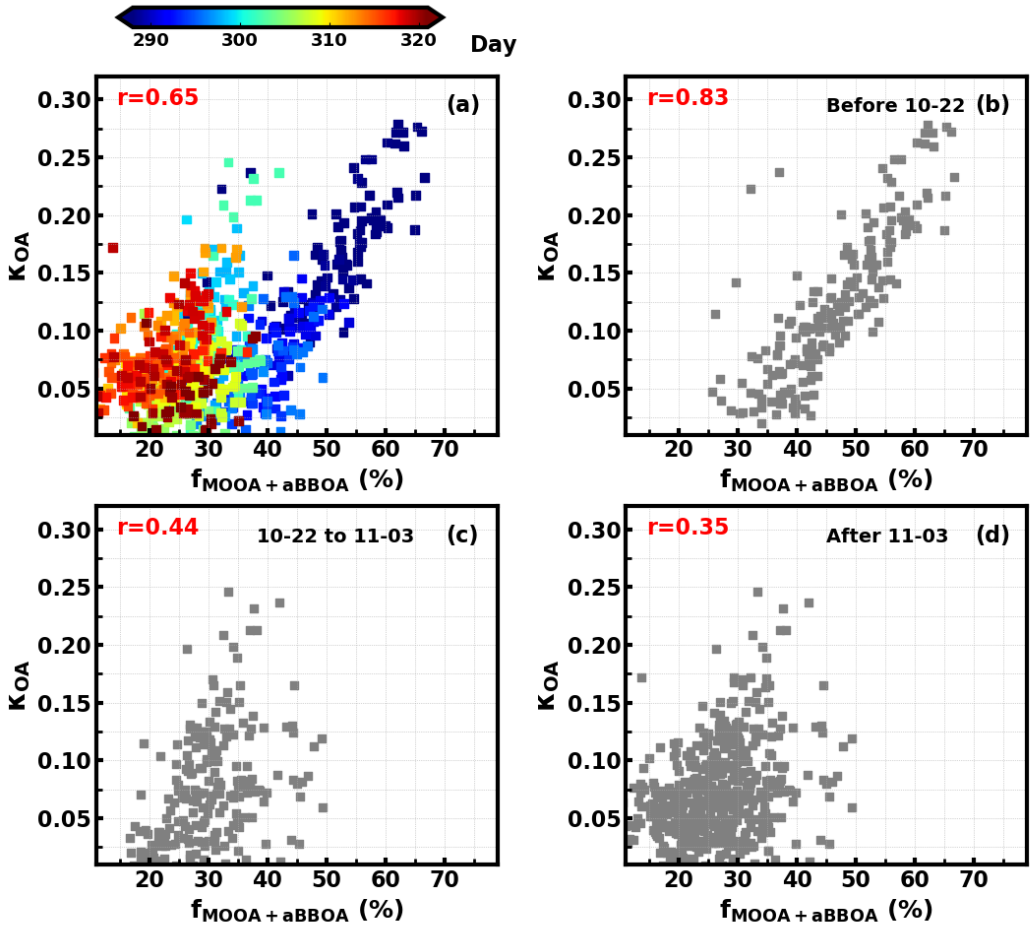

Figure 7. Relationships between κ_{OA} and $f_{MOOA+aBBOA}$ during (a) the entire observation period; （b）10-12 to 10-22; (c) 10-23 to 11-02; (d) 11-03 to 11-17. Colors of scatter points in (a) represents day of the year.

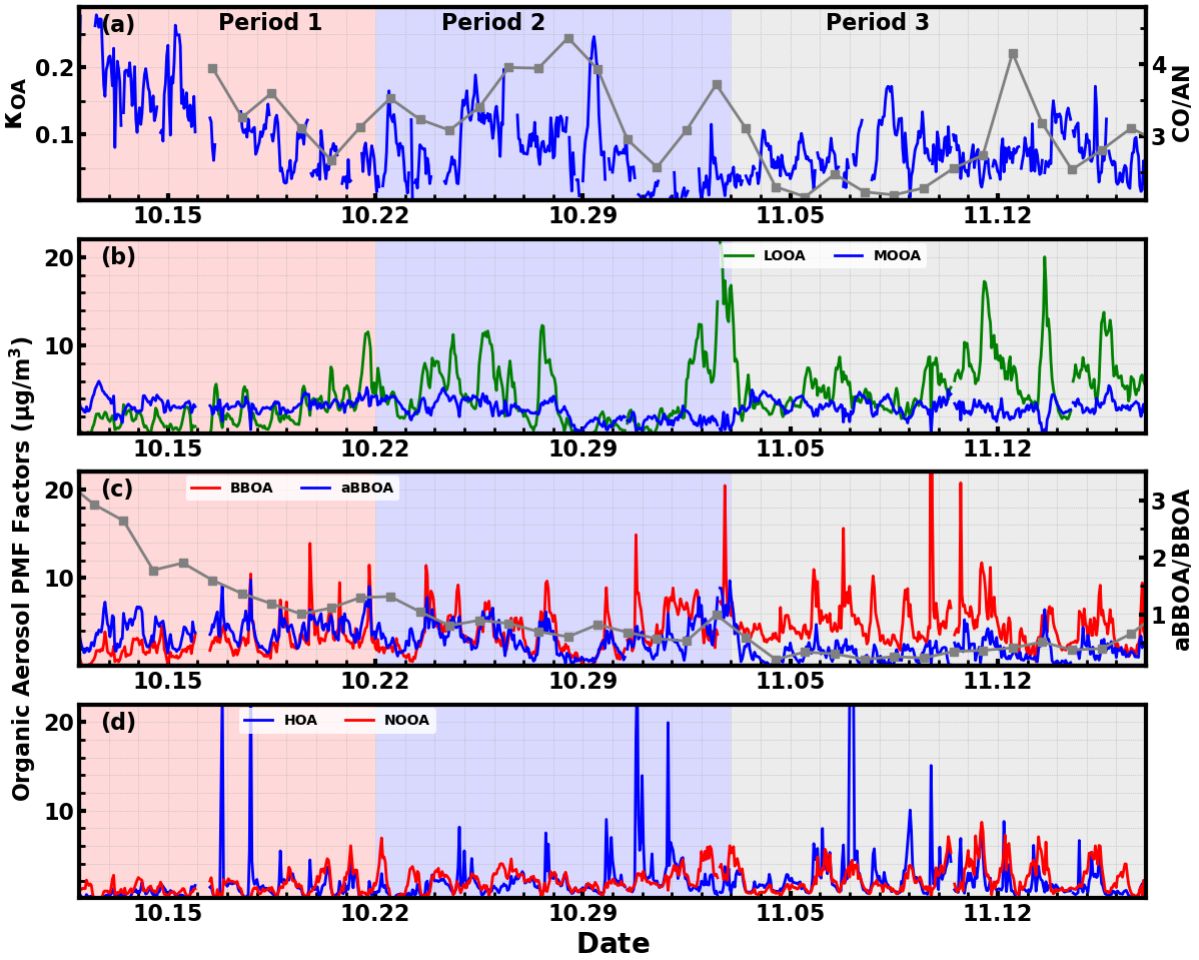

Figure 8. Time series of **(a)** derived κ_{OA} and the right y-axis represent the ratio between CO and AN (acetonitrile); **(b)** LOOA and MOOA; **(c)** BBOA and aged BBOA, and the right axis represents the ratio between aBBOA/BBOA; **(d)** HOA and NOOA

CO and acetonitrile are highly associated with biomass burning and are often used as indicators of biomass burning events, and the ratio between them can somehow indicate the emission profile changes of biomass burning thus the primary VOC profile changes. The time series of the ratio between CO and acetonitrile (Fig.~~7a~~8a) differs much during the three periods, especially for the second and the third period. This difference suggests that although the biomass burning event continued, their emission profiles associated with the burning fuels and conditions likely changed a lot, indicating that aBBOA precursors might have changed during different agricultural activities, thus changing their formation pathways as well as their chemical and physical properties. Other than the aBBOA property changes, changes in OA factor contributions (for example, relative contributions of OA factors other than MOOA and aBBOA) may also impact on the relationship between κ_{OA} and $f_{\mathrm{MOOA+aBBOA}}$. Also, the chemical and physical properties of Night-OA and LOOA together with the VOC profile can also

have changed.

In general, the results shown here deliver the following key messages: (1) Although the O/C failed to describe variations in κ_{OA}, variations of OA factors that are more related to VOC sources or OA formation pathways could sometimes be found to explain the κ_{OA} variations; (2) MOOA , being highly oxygenated and associated with regional air mass, was the most important component that enhanced κ_{OA}, which is consistent with current understandings, i.e., organic aerosol aging processes have significant effects on κ_{OA}. However, the κ_{OA} of secondary organic aerosol does not depends on their O/C (contrary effects of aBBOA and LOOA on κ_{OA}); (3) Organic aerosol hygroscopicity of SOA associated with similar sources might differ much under different conditions (effects of aBBOA on κ_{OA} differ much during different periods).

These messages might be instructive to the parameterization of κ_{OA} in the following ways: (1) We might relate κ_{OA} to VOC precursors in laboratory studies, but the laboratory derived empirical relationship will likely fail in application of ambient aerosols due to the formation pathway or the existence of other VOC precursors might result in different chemical properties of ambient formed SOA, such as functional groups, from the laboratory case; (2) It seems more plausible to find parameters other than O/C ratio to parameterize κ_{OA}, which should be independent of sources and associated with the physical properties of OA~~.~~, such as volatility (Kuwata et al., 2007;Asa-Awuku et al., 2009;Frosch et al., 2013;Kostenidou et al., 2018). Overall, these results further highlighted that κ_{OA} parameterizations can be quite difficult and requires a lot of future efforts.

5 Conclusions

In this study, a field campaign was conducted to characterize κ_{OA} with high time resolution for the first time at a rural site in the PRD region. The observation results showed that both typical NO_3 night chemistry (indicated by ~~quick nighttime nitrate formation,~~ extremely low nighttime NO concentration and quick nighttime O_3 concentration decrease) and strong daytime photochemical chemistry (indicated by high daytime O_3 concentration) prevailed during this field campaign. SOA dominated OA mass (mass fraction >70% on average), which provided us a unique opportunity to investigate influences of SOA formation on variations in organic aerosol hygroscopicity parameter κ_{OA}. Six OA factors were resolved by the AMS PMF analysis, including two primary OA factors HOA and BBOA and other four secondary OA factors MOOA, LOOA, aBBOA and Night-OA. The results

demonstrated that mass increase in both two primary OA factors had negative effects on $\boldsymbol{\kappa_{OA}}$, which is consistent with current understandings that POA components have quite low hygroscopicity (usually assumed as hydrophilic), while SOA components had distinct effects on $\boldsymbol{\kappa_{OA}}$. MOOA with the highest average O/C of 1 was the most important factor that droves the increase of $\boldsymbol{\kappa_{OA}}$, probably related with regional air mass and local production contributes small. However, LOOA with average O/C slightly lower than that of MOOA (O/C ~ 0.72), whose mass concentration increased dramatically during daytime due to local production, had negative effects on $\boldsymbol{\kappa_{OA}}$. Surprisingly, aBBOA with similar diurnal patterns to that of LOOA, also formed quickly during daytime, but displayed much lower O/C (0.39), exerting positive effects on $\boldsymbol{\kappa_{OA}}$. In addition, $\boldsymbol{\kappa_{OA}}$ revealed weak negative correlation to Night-OA fraction, which increased during nighttime probably due to the NO_3 nighttime chemistry. This finding is in general consistent with results of Suda et al. (2014) that the addition of NO_3 radical would exert negative impacts on $\boldsymbol{\kappa_{OA}}$. As a result, the contrasting effects of LOOA and aBBOA on $\boldsymbol{\kappa_{OA}}$ resulted in the weak correlation coefficient between $\boldsymbol{\kappa_{OA}}$ and O/C. $\boldsymbol{\kappa_{OA}}$ was mostly associated with mass fractions of MOOA with highest O/C although its O/C is only a little higher than that of LOOA, which gave rise to the weak but positive relationship between $\boldsymbol{\kappa_{OA}}$ and O/C.

In general, the results presented in this study demonstrate that the O/C failed to describe variations in $\boldsymbol{\kappa_{OA}}$, however, SOA factors with different VOC sources or from different OA formation pathways might have discrepant influences on the $\boldsymbol{\kappa_{OA}}$. The contrasting effects of LOOA and aBBOA on $\boldsymbol{\kappa_{OA}}$ demonstrated that VOC precursors from diverse sources and different SOA formation processes may result in SOA with different chemical composition, functional properties as well as microphysical structure, consequently influencing SOA hygroscopicity. On top of that, the hygroscopicity of SOA associated with similar sources might also differ much during different emission and atmospheric conditions. These results demonstrate that we might relate $\boldsymbol{\kappa_{OA}}$ to VOC precursors in laboratory studies, but the laboratory derived empirical relationships will likely fail in their application to ambient aerosols due to the more complex formation pathways or the existence of other VOC precursors in the ambient atmosphere, and thus difficult to apply in models. Overall, these results further highlighted that $\boldsymbol{\kappa_{OA}}$ parameterizations are quite complex, and it is important to conduct more researches on $\boldsymbol{\kappa_{OA}}$ characterization under different meteorological and source conditions, and examine its relationship with OA and VOC precursor profiles to reach a better characterization and come up with a more appropriate parameterization approach for chemical and climate models.

Data availability. The data used in this study are available from the corresponding author upon request Shan Huang (shanhuang_eci@jnu.edu.cn) and Min Shao (mshao@jnu.edu.cn)

Competing interests. The authors declare that they have no conflict of interest.

Author Contributions. YK and SH designed the aerosol experiments. YK conceived this research and wrote the manuscript together with SH. YK, BL and BX conducted aerosol light scattering enhancement factor measurements. QS, WC, WL, SH and WH conducted the SP-AMS measurements. MC, YK and SH conducted the particle number size distribution measurements. MS and BY planned and funded this campaign. YP collected and managed criterial pollutants and meteorological parameters from Heshan supersite. PZ provided the humidified nephelometer system and contributed to discussions and revisions of the manuscript. DC and DY provided authority of conducting the campaign in Heshan supersite and gave data availability from the site. All other coauthors have contributed to this paper in different ways.

Acknowledgments

This work is supported by the National Natural Science Foundation of China (grant No. 41805109, 41807302), National Key Research and Development Program of China (grant No. 2017YFC0212803, 2016YFC0202206, 2017YFB0503901), Key-Area Research and Development Program of Guangdong Province (grant No. 2019B110206001), Guangdong Natural Science Foundation (grant No. 2018A030313384), Special Fund Project for Science and Technology Innovation Strategy of Guangdong Province (grant No.2019B121205004), Guangdong Natural Science Funds for Distinguished Young Scholar (grant No. 2018B030306037) and Guangdong Innovative and Entrepreneurial Research Team Program (grant No. 2016ZT06N263).

References

Alfarra, M. R., Good, N., Wyche, K. P., Hamilton, J. F., Monks, P. S., Lewis, A. C., and McFiggans, G.: Water uptake is independent of the inferred composition of secondary aerosols derived from multiple biogenic VOCs, Atmos. Chem. Phys., 13, 11769-11789, 10.5194/acp-13-11769-2013, 2013.

Asa-Awuku, A., Engelhart, G. J., Lee, B. H., Pandis, S. N., and Nenes, A.: Relating CCN activity, volatility, and droplet growth kinetics of β-caryophyllene secondary organic aerosol, Atmos. Chem. Phys., 9, 795-812, 10.5194/acp-9-795-2009, 2009.

Bertrand, A., Stefenelli, G., Jen, C. N., Pieber, S. M., Bruns, E. A., Ni, H., Temime-Roussel, B., Slowik, J. G., Goldstein, A. H., El Haddad, I., Baltensperger, U., Prévôt, A. S. H., Wortham, H., and Marchand, N.: Evolution of the chemical fingerprint of biomass burning organic aerosol during aging, Atmos. Chem. Phys., 18, 7607-7624, 10.5194/acp-18-7607-2018, 2018.

Canagaratna, M. R., Jayne, J. T., Jimenez, J. L., Allan, J. D., Alfarra, M. R., Zhang, Q., Onasch, T. B., Drewnick, F., Coe, H., Middlebrook, A., Delia, A., Williams, L. R., Trimborn, A. M., Northway, M. J., DeCarlo, P. F., Kolb, C. E., Davidovits, P., and Worsnop, D. R.: Chemical and microphysical characterization of ambient aerosols with the aerodyne aerosol mass spectrometer, Mass Spectrom. Rev., 26, 185-222, 10.1002/mas.20115, 2007.

Cerully, K. M., Bougiatioti, A., Hite Jr, J. R., Guo, H., Xu, L., Ng, N. L., Weber, R., and Nenes, A.: On the link between hygroscopicity, volatility, and oxidation state of ambient and water-soluble aerosols in the southeastern United States, Atmos. Chem. Phys., 15, 8679-8694, 10.5194/acp-15-8679-2015, 2015.

Chen, J., Zhao, C. S., Ma, N., and Yan, P.: Aerosol hygroscopicity parameter derived from the light scattering enhancement factor measurements in the North China Plain, Atmos. Chem. Phys. Discuss., 14, 3459-3497, 10.5194/acpd-14-3459-2014, 2014.

Deng, Y., Yai, H., Fujinari, H., Kawana, K., Nakayama, T., and Mochida, M.: Diurnal variation and size dependence of the hygroscopicity of organic aerosol at a forest site in Wakayama, Japan: their relationship to CCN concentrations, Atmos. Chem. Phys., 19, 5889-5903, 10.5194/acp-19-5889-2019, 2019.

Frosch, M., Bilde, M., Nenes, A., Praplan, A. P., Jurányi, Z., Dommen, J., Gysel, M., Weingartner, E., and Baltensperger, U.: CCN activity and volatility of β-caryophyllene secondary organic aerosol, Atmos. Chem. Phys., 13, 2283-2297, 10.5194/acp-13-2283-2013, 2013.

Gunthe, S. S., Rose, D., Su, H., Garland, R. M., Achtert, P., Nowak, A., Wiedensohler, A., Kuwata, M., Takegawa, N., Kondo, Y., Hu, M., Shao, M., Zhu, T., Andreae, M. O., and Pöschl, U.: Cloud condensation nuclei (CCN) from fresh and aged air pollution in the megacity region of Beijing, Atmos. Chem. Phys., 11, 11023-11039, 10.5194/acp-11-11023-2011, 2011.

Guo, J., Zhou, S., Cai, M., Zhao, J., Song, W., Zhao, W., Hu, W., Sun, Y., He, Y., Yang, C., Xu, X., Zhang, Z., Cheng, P., Fan, Q., Hang, J., Fan, S., Wang, X., and Wang, X.: Characterization of submicron particles by time-of-flight aerosol chemical speciation monitor (ToF-ACSM) during wintertime: aerosol composition, sources, and chemical processes in Guangzhou, China, Atmospheric Chemistry and Physics, 20, 7595-7615, 10.5194/acp-20-7595-2020, 2020.

Gysel, M., Crosier, J., Topping, D. O., Whitehead, J. D., Bower, K. N., Cubison, M. J., Williams, P. I., Flynn, M. J., McFiggans, G. B., and Coe, H.: Closure study between chemical composition and hygroscopic growth of aerosol particles during TORCH2, Atmos. Chem. Phys., 7, 6131-6144, 10.5194/acp-7-6131-2007, 2007.

Hong, J., Xu, H., Tan, H., Yin, C., Hao, L., Li, F., Cai, M., Deng, X., Wang, N., Su, H., Cheng, Y., Wang, L., Petäjä, T., and Kerminen, V. M.: Mixing state and particle hygroscopicity of organic-dominated aerosols over the Pearl River Delta region in China, Atmos. Chem. Phys., 18, 14079-14094, 10.5194/acp-18-14079-2018, 2018.

Jimenez, J. L., Canagaratna, M. R., Donahue, N. M., Prevot, A. S. H., Zhang, Q., Kroll, J. H., DeCarlo, P. F., Allan, J. D., Coe, H., Ng, N. L., Aiken, A. C., Docherty, K. S., Ulbrich, I. M., Grieshop, A. P., Robinson, A. L., Duplissy, J., Smith, J. D., Wilson, K. R., Lanz, V. A., Hueglin, C., Sun, Y. L., Tian, J., Laaksonen, A., Raatikainen, T., Rautiainen, J., Vaattovaara, P., Ehn, M., Kulmala, M., Tomlinson, J. M., Collins, D. R., Cubison, M. J., Dunlea, J., Huffman, J. A., Onasch, T. B., Alfarra, M. R., Williams, P. I.,

Bower, K., Kondo, Y., Schneider, J., Drewnick, F., Borrmann, S., Weimer, S., Demerjian, K., Salcedo, D., Cottrell, L., Griffin, R., Takami, A., Miyoshi, T., Hatakeyama, S., Shimono, A., Sun, J. Y., Zhang, Y. M., Dzepina, K., Kimmel, J. R., Sueper, D., Jayne, J. T., Herndon, S. C., Trimborn, A. M., Williams, L. R., Wood, E. C., Middlebrook, A. M., Kolb, C. E., Baltensperger, U., and Worsnop, D. R.: Evolution of Organic Aerosols in the Atmosphere, Science, 326, 1525-1529, 10.1126/science.1180353, 2009.

Jin, X., Wang, Y., Li, Z., Zhang, F., Xu, W., Sun, Y., Fan, X., Chen, G., Wu, H., Ren, J., Wang, Q., and Cribb, M.: Significant contribution of organics to aerosol liquid water content in winter in Beijing, China, Atmos. Chem. Phys., 20, 901-914, 10.5194/acp-20-901-2020, 2020.

Jing, B., Wang, Z., Tan, F., Guo, Y., Tong, S., Wang, W., Zhang, Y., and Ge, M.: Hygroscopic behavior of atmospheric aerosols containing nitrate salts and water-soluble organic acids, Atmospheric Chemistry and Physics, 18, 5115-5127, 10.5194/acp-18-5115-2018, 2018.

Koehler, K. A., Kreidenweis, S. M., DeMott, P. J., Petters, M. D., Prenni, A. J., and Carrico, C. M.: Hygroscopicity and cloud droplet activation of mineral dust aerosol, Geophysical Research Letters, 36, 10.1029/2009GL037348, 2009.

Kostenidou, E., Karnezi, E., Hite Jr, J. R., Bougiatioti, A., Cerully, K., Xu, L., Ng, N. L., Nenes, A., and Pandis, S. N.: Organic aerosol in the summertime southeastern United States: components and their link to volatility distribution, oxidation state and hygroscopicity, Atmos. Chem. Phys., 18, 5799-5819, 10.5194/acp-18-5799-2018, 2018.

Kuang, Y., Zhao, C., Tao, J., Bian, Y., Ma, N., and Zhao, G.: A novel method for deriving the aerosol hygroscopicity parameter based only on measurements from a humidified nephelometer system, Atmos. Chem. Phys., 17, 6651-6662, 10.5194/acp-17-6651-2017, 2017.

Kuang, Y., He, Y., Xu, W., Zhao, P., Cheng, Y., Zhao, G., Tao, J., Ma, N., Su, H., Zhang, Y., Sun, J., Cheng, P., Yang, W., Zhang, S., Wu, C., Sun, Y., and Zhao, C.: Distinct diurnal variation in organic aerosol hygroscopicity and its relationship with oxygenated organic aerosol, Atmos. Chem. Phys., 20, 865-880, 10.5194/acp-20-865-2020, 2020a.

Kuang, Y., Xu, W., Tao, J., Ma, N., Zhao, C., and Shao, M.: A Review on Laboratory Studies and Field Measurements of Atmospheric Organic Aerosol Hygroscopicity and Its Parameterization Based on Oxidation Levels, Current Pollution Reports, 10.1007/s40726-020-00164-2, 2020b.

Kuwata, M., Kondo, Y., Mochida, M., Takegawa, N., and Kawamura, K.: Dependence of CCN activity of less volatile particles on the amount of coating observed in Tokyo, Journal of Geophysical Research: Atmospheres, 112, https://doi.org/10.1029/2006JD007758, 2007.

Kuwata, M., Zorn, S. R., and Martin, S. T.: Using Elemental Ratios to Predict the Density of Organic Material Composed of Carbon, Hydrogen, and Oxygen, Environmental science & technology, 46, 787-794, 10.1021/es202525q, 2012.

Lambe, A. T., Onasch, T. B., Massoli, P., Croasdale, D. R., Wright, J. P., Ahern, A. T., Williams, L. R., Worsnop, D. R., Brune, W. H., and Davidovits, P.: Laboratory studies of the chemical composition and cloud condensation nuclei (CCN) activity of secondary organic aerosol (SOA) and oxidized primary organic aerosol (OPOA), Atmos. Chem. Phys., 11, 8913-8928, 10.5194/acp-11-8913-2011, 2011.

Lathem, T. L., Beyersdorf, A. J., Thornhill, K. L., Winstead, E. L., Cubison, M. J., Hecobian, A., Jimenez, J. L., Weber, R. J., Anderson, B. E., and Nenes, A.: Analysis of CCN activity of Arctic aerosol and Canadian biomass burning during summer 2008, Atmos. Chem. Phys., 13, 2735-2756, 10.5194/acp-13-2735-2013, 2013.

Li, X., Song, S., Zhou, W., Hao, J., Worsnop, D. R., and Jiang, J.: Interactions between aerosol organic components and liquid water content during haze episodes in Beijing, Atmos. Chem. Phys., 19, 12163-12174, 10.5194/acp-19-12163-2019, 2019.

Liu, H. J., Zhao, C. S., Nekat, B., Ma, N., Wiedensohler, A., van Pinxteren, D., Spindler, G., Müller, K., and Herrmann, H.: Aerosol hygroscopicity derived from size-segregated chemical composition and its parameterization in the North China Plain, Atmos. Chem. Phys., 14, 2525-2539, 10.5194/acp-14-2525-2014, 2014.

Liu, P., Song, M., Zhao, T., Gunthe, S. S., Ham, S., He, Y., Qin, Y. M., Gong, Z., Amorim, J. C., Bertram, A. K., and Martin, S. T.: Resolving the mechanisms of hygroscopic growth and cloud condensation nuclei activity for organic particulate matter,

Nature communications, 9, 4076, 10.1038/s41467-018-06622-2, 2018.
Liu, X., and Wang, J.: How important is organic aerosol hygroscopicity to aerosol indirect forcing?, Environmental Research Letters, 5, 044010, 10.1088/1748-9326/5/4/044010, 2010.
Luo, Q., Hong, J., Xu, H., Han, S., Tan, H., Wang, Q., Tao, J., Ma, N., Cheng, Y., and Su, H.: Hygroscopicity of amino acids and their effect on the water uptake of ammonium sulfate in the mixed aerosol particles, The Science of the total environment, 734, 139318, 10.1016/j.scitotenv.2020.139318, 2020.
Ma, N., Zhao, C. S., Nowak, A., Müller, T., Pfeifer, S., Cheng, Y. F., Deng, Z. Z., Liu, P. F., Xu, W. Y., Ran, L., Yan, P., Göbel, T., Hallbauer, E., Mildenberger, K., Henning, S., Yu, J., Chen, L. L., Zhou, X. J., Stratmann, F., and Wiedensohler, A.: Aerosol optical properties in the North China Plain during HaChi campaign: an in-situ optical closure study, Atmos. Chem. Phys., 11, 5959-5973, 10.5194/acp-11-5959-2011, 2011.
Marsh, A., Miles, R. E. H., Rovelli, G., Cowling, A. G., Nandy, L., Dutcher, C. S., and Reid, J. P.: Influence of organic compound functionality on aerosol hygroscopicity: dicarboxylic acids, alkyl-substituents, sugars and amino acids, Atmospheric Chemistry and Physics, 17, 5583-5599, 10.5194/acp-17-5583-2017, 2017.
Massoli, P., Lambe, A. T., Ahern, A. T., Williams, L. R., Ehn, M., Mikkilä, J., Canagaratna, M. R., Brune, W. H., Onasch, T. B., Jayne, J. T., Petäjä, T., Kulmala, M., Laaksonen, A., Kolb, C. E., Davidovits, P., and Worsnop, D. R.: Relationship between aerosol oxidation level and hygroscopic properties of laboratory generated secondary organic aerosol (SOA) particles, Geophysical Research Letters, 37, 10.1029/2010gl045258, 2010.
Middlebrook, A. M., Bahreini, R., Jimenez, J. L., and Canagaratna, M. R.: Evaluation of Composition-Dependent Collection Efficiencies for the Aerodyne Aerosol Mass Spectrometer using Field Data, Aerosol Science and Technology, 46, 258-271, 10.1080/02786826.2011.620041, 2012.
Onasch, T. B., Trimborn, A., Fortner, E. C., Jayne, J. T., Kok, G. L., Williams, L. R., Davidovits, P., and Worsnop, D. R.: Soot Particle Aerosol Mass Spectrometer: Development, Validation, and Initial Application, Aerosol Sci. Tech., 46, 804-817, 10.1080/02786826.2012.663948, 2012.
Paatero, P., and Tapper, U.: Positive matrix factorization: A non-negative factor model with optimal utilization of error estimates of data values, Environmetrics, 5, 111-126, 10.1002/env.3170050203, 1994.
Paatero, P.: Least squares formulation of robust non-negative factor analysis, Chemometr Intell Lab, 37, 23-35, 10.1016/S0169-7439(96)00044-5, 1997.
Peng, C., Gu, W., Li, R., Lin, Q., Ma, Q., Jia, S., Krishnan, P., Wang, X., and Tang, M.: Large Variations in Hygroscopic Properties of Unconventional Mineral Dust, ACS Earth and Space Chemistry, 4, 1823-1830, 10.1021/acsearthspacechem.0c00219, 2020.
Petters, M. D., and Kreidenweis, S. M.: A single parameter representation of hygroscopic growth and cloud condensation nucleus activity, Atmospheric Chemistry and Physics, 7, 1961-1971, 2007.
Petters, S. S., Pagonis, D., Claflin, M. S., Levin, E. J. T., Petters, M. D., Ziemann, P. J., and Kreidenweis, S. M.: Hygroscopicity of Organic Compounds as a Function of Carbon Chain Length and Carboxyl, Hydroperoxy, and Carbonyl Functional Groups, The Journal of Physical Chemistry A, 121, 5164-5174, 10.1021/acs.jpca.7b04114, 2017.
Rastak, N., Pajunoja, A., Acosta Navarro, J. C., Ma, J., Song, M., Partridge, D. G., Kirkevåg, A., Leong, Y., Hu, W. W., Taylor, N. F., Lambe, A., Cerully, K., Bougiatioti, A., Liu, P., Krejci, R., Petäjä, T., Percival, C., Davidovits, P., Worsnop, D. R., Ekman, A. M. L., Nenes, A., Martin, S., Jimenez, J. L., Collins, D. R., Topping, D. O., Bertram, A. K., Zuend, A., Virtanen, A., and Riipinen, I.: Microphysical explanation of the RH-dependent water affinity of biogenic organic aerosol and its importance for climate, Geophysical Research Letters, 44, 5167-5177, 10.1002/2017gl073056, 2017.
Rickards, A. M. J., Miles, R. E. H., Davies, J. F., Marshall, F. H., and Reid, J. P.: Measurements of the Sensitivity of Aerosol Hygroscopicity and the κ Parameter to the O/C Ratio, The Journal of Physical Chemistry A, 117, 14120-14131, 10.1021/jp407991n, 2013.
Suda, S. R., Petters, M. D., Yeh, G. K., Strollo, C., Matsunaga, A., Faulhaber, A., Ziemann, P. J., Prenni, A. J., Carrico, C. M.,

Sullivan, R. C., and Kreidenweis, S. M.: Influence of Functional Groups on Organic Aerosol Cloud Condensation Nucleus Activity, Environmental science & technology, 48, 10182-10190, 10.1021/es502147y, 2014.

Ulbrich, I. M., Canagaratna, M. R., Zhang, Q., Worsnop, D. R., and Jimenez, J. L.: Interpretation of organic components from Positive Matrix Factorization of aerosol mass spectrometric data, Atmos. Chem. Phys., 9, 2891-2918, 10.5194/acp-9-2891-2009, 2009.

Wang, Y., Hu, M., Wang, Y., Zheng, J., Shang, D., Yang, Y., Liu, Y., Li, X., Tang, R., Zhu, W., Du, Z., Wu, Y., Guo, S., Wu, Z., Lou, S., Hallquist, M., and Yu, J. Z.: The formation of nitro-aromatic compounds under high NOx and anthropogenic VOC conditions in urban Beijing, China, Atmos. Chem. Phys., 19, 7649-7665, 10.5194/acp-19-7649-2019, 2019.

Wu, Z. J., Poulain, L., Henning, S., Dieckmann, K., Birmili, W., Merkel, M., van Pinxteren, D., Spindler, G., Müller, K., Stratmann, F., Herrmann, H., and Wiedensohler, A.: Relating particle hygroscopicity and CCN activity to chemical composition during the HCCT-2010 field campaign, Atmos. Chem. Phys., 13, 7983-7996, 10.5194/acp-13-7983-2013, 2013.

Wu, Z. J., Zheng, J., Shang, D. J., Du, Z. F., Wu, Y. S., Zeng, L. M., Wiedensohler, A., and Hu, M.: Particle hygroscopicity and its link to chemical composition in the urban atmosphere of Beijing, China, during summertime, Atmos. Chem. Phys., 16, 1123-1138, 10.5194/acp-16-1123-2016, 2016.

Xu, W., Kuang, Y., Bian, Y., Liu, L., Li, F., Wang, Y., Xue, B., Luo, B., Huang, S., Yuan, B., Zhao, P., and Shao, M.: Current Challenges in Visibility Improvement in Southern China, Environmental Science & Technology Letters, 7, 395-401, 10.1021/acs.estlett.0c00274, 2020.

Yeung, M. C., Lee, B. P., Li, Y. J., and Chan, C. K.: Simultaneous HTDMA and HR-ToF-AMS measurements at the HKUST Supersite in Hong Kong in 2011, Journal of Geophysical Research: Atmospheres, 119, 9864-9883, 10.1002/2013JD021146, 2014.

Zhao, D. F., Buchholz, A., Kortner, B., Schlag, P., Rubach, F., Fuchs, H., Kiendler-Scharr, A., Tillmann, R., Wahner, A., Watne, Å. K., Hallquist, M., Flores, J. M., Rudich, Y., Kristensen, K., Hansen, A. M. K., Glasius, M., Kourtchev, I., Kalberer, M., and Mentel, T. F.: Cloud condensation nuclei activity, droplet growth kinetics, and hygroscopicity of biogenic and anthropogenic secondary organic aerosol (SOA), Atmospheric Chemistry and Physics, 16, 1105-1121, 10.5194/acp-16-1105-2016, 2016.

Zhou, W., Xu, W., Kim, H., Zhang, Q., Fu, P., Worsnop, D. R., and Sun, Y.: A review of aerosol chemistry in Asia: insights from aerosol mass spectrometer measurements, Environmental Science: Processes & Impacts, 10.1039/D0EM00212G, 2020a.

Zhou, W., Xu, W., Kim, H., Zhang, Q., Fu, P., Worsnop, D. R., and Sun, Y.: A review of aerosol chemistry in Asia: insights from aerosol mass spectrometer measurements, Environmental Science: Processes & Impacts, 22, 1616-1653, 10.1039/D0EM00212G, 2020b.